Tenth International Conference on Computational Fluid Dynamics (ICCFD10), Barcelona, Spain, July 9-13, 2018

ICCFD10-045

Application of Computational Fluid Dynamics to the Flow Mixing and Heat Transfer in Rod Bundle

W. K. In*, K. G. Lee*, **, and C. H. Shin*
Corresponding author: wkin@kaeri.re.kr

* Korea Atomic Energy Research Institute, Rep. of Korea
** University of Science and Technology, Rep. of Korea.

Abstract: A Computational Fluid Dynamics analysis is performed to predict flow mixing and heat transfer in a 4x4 rod bundle with a mixing-vane grid. The diameter of the rod is 25.4 mm and the pitch-to-diameter ratio is 1.35. The average flow velocity of water is 1.5 m/s and the surface heat flux in a heated rod is 104 kW/m^2. The CFD analysis predicted a swirl inside the subchannel and crossflow between adjacent subcahnnels, which were generated by the mixing-vane grid. The CFD predictions of axial and lateral velocity distributions agree with the experimental results well. The cold and hot spots were predicted in a heated rod downstream of the mixing vane owing to a non-uniform flow mixing. The CFD prediction of the wall temperature in a heated rod shows a somewhat large difference with the measured one in a narrow gap region, and far downstream of the vane grid.

Keywords: Computational Fluid Dynamics, Rod Bundle, Mixing-vane grid, Pitch-to-diameter ratio (P/D), Subchannel.

1 Introduction

The fuel assembly in a nuclear reactor is a rod bundle in which the coolant (water) flows through the subchannels formed between fuel rods. The fuel assembly loaded in pressurized water reactor (PWR) is typically a 16x16 or 17x17 square array of fuel rods, as shown in Figure 1. The diameter of the fuel rod (D) is 9.5-9.8 mm, and the ratio of rod pitch and diameter (*P/D*) is 1.33-1.35. The spacer grid is used to support the fuel rods in the right position for the integrity of the fuel assembly. The coolant (water) flows axially through the subchannel formed between the rods. Because the spacer grid affects the coolant flow distribution in the fuel bundle, the spacer geometry has a strong influence on the thermal-hydraulic performance of a fuel assembly, such as the critical heat flux (CHF) and pressure drop. A mixing-vane grid was also developed to enhance the coolant mixing and heat transfer in a fuel-rod bundle. It is therefore important to understand the flow mixing pattern and heat transfer in a nuclear fuel assembly for the reactor safety and reliable operation.

There have been many experimental and numerical studies on the flow mixing and heat transfer downstream of the mixing-vane grid in a rod bundle geometry. Shen [1] and Yang and Chung [2] performed an experiment to examine the flow mixing and turbulent characteristics in a rod bundle with a split-vane spacer grid. McClusky et al. [3, 4] measured the lateral flow field in typical subchannels of a rod bundle with a split-vane grid. There have also been many numerical works on evaluating the rod-bundle flow mixing caused by a split-vane grid [5-7]. Holloway et al. [8, 9] and Conner et al. [10] carried out an experimental study to investigate the effects of a split-vane grid on the heat transfer of the rod bundles.

The International Atomic Energy Agency (IAEA) organized a Coordinated Research Project

(CRP) on the application of Computational Fluid Dynamics (CFD) codes to a nuclear power plant (NPP) design. The rod-bundle tests carried out by the Korea Atomic Energy Research Institute (KAERI) were chosen as one of the benchmark tests for the verification and validation of the CFD method in this IAEA CRP. KAERI provided CFD-grade experimental data from the PIV (Particle Image Velocimetry) and LDV (Laser Doppler Velocimetry) measurements of flow mixing and heat transfer in a 4x4 rod bundle with a twist-vane grid [11, 12]. The bundle-flow velocity is 1.5 m/s and the surface heat flux in a heated rod is 104 kW/m^2. The working fluid is water in room temperature.

A CFD analysis was performed to simulate the KAERI bundle experiments (isothermal and thermal tests) using the commercial CFD codes, ANSYS CFX [13] and STAR-CCM+ [14]. The CFD simulation of the isothermal bundle test calculated the axial and lateral velocity distributions in the central subchannel of a 4x4 rod bundle. The CFD analysis for thermal bundle test predicted the circumferential variation of wall temperature in a heated rod. The CFD predictions are compared with the experimental results for the isothermal and thermal tests using a 4x4 rod bundle with the mixing-vane grid. This CFD analysis also investigated the effects of the mesh type (tetrahedral vs. polyhedral cells) and turbulence model.

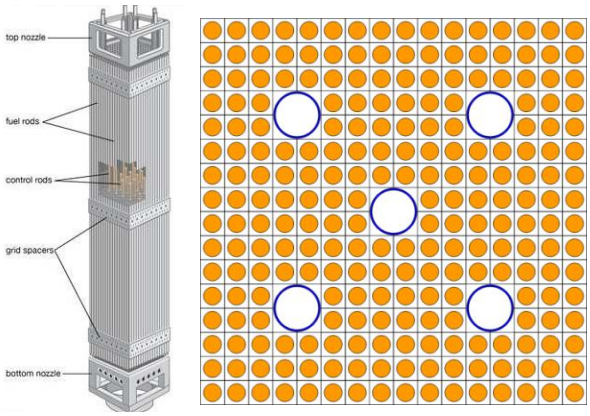

Figure 1: Schematic of fuel assembly in pressurized water reactor.

2 Rod Bundle Experiments

2.1 Flow-mixing Experiment

The Omni Flow Experimental Loop (OFEL) has been built to measure the thermal-hydraulic characteristics of a rod bundle flow. OFEL consists of a test section with a rod bundle geometry, a centrifugal water pump, a water storage tank and a flow meter, as shown in Figure 2. The water temperature for testing is controlled by the immersion cartridge heater, and by a heat exchanger of air cooling connected to the water storage tank. Using a centrifugal pump, the water flows from the reservoir to the plenum at the lower part of the vertical test section. The water flow rate is controlled by the VFD (Variable Frequency Drive), and is measured using the mass and turbine flow meters.

To measure the water temperature, a T-type thermocouple (Omega) is installed in the inlet plenum. All experimental data are collected using a commercial data acquisition system. As a working fluid, de-mineralized water is used. To measure the flow velocities within the rod bundle, both PIV and LDV techniques are employed. For the PIV system (Dantec), the laser has dual cavities. For each cavity, the power, pulse rate and wavelength are 20 mJ, 1 kHz and 527 nm, respectively. A high-speed camera (Speed Sense 9072) can provide up to 2190 fps (frames/sec) at full resolution of a 1280×800 pixel matrix. For the LDV system set-up, the laser power and wavelength are 130 mW and 660 nm, respectively. The PIV set-up is illustrated in Fig. 3.

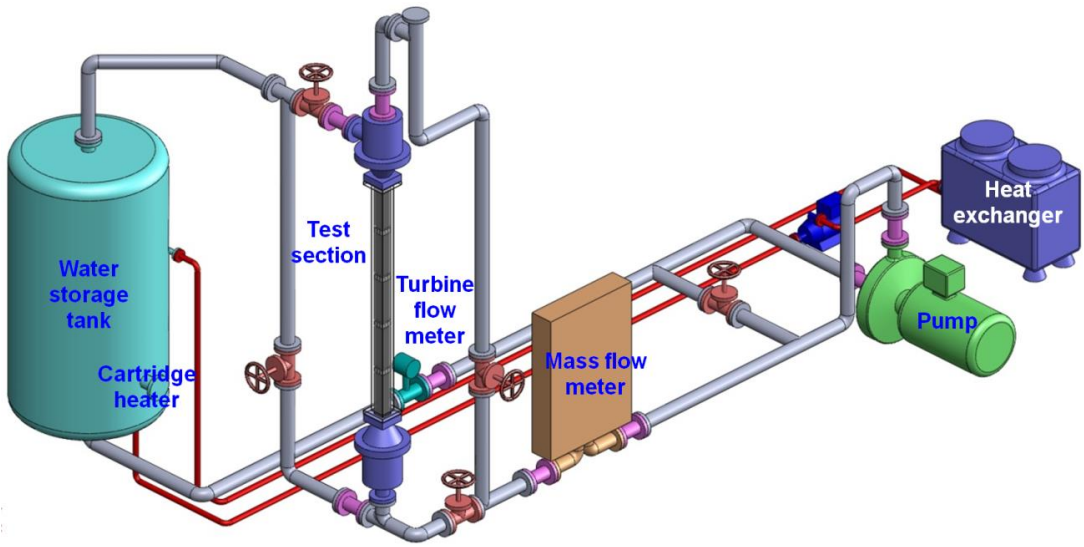

Figure 2: Schematic of the OFEL test loop.

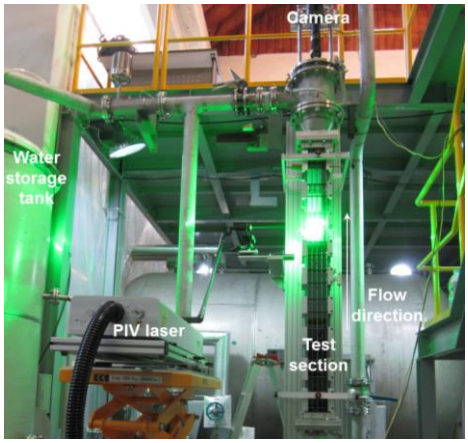

Figure 3: Setup of the PIV system in OFEL test loop.

The test section consists of a square housing, holder, rod bundle, fixing plate, rod support, and spacer grid with mixing vanes of a generic design, as shown in Fig. 4. The dimensions of the square housings are 142 mm × 142 mm. The cylindrical rod is 2000 mm in length and 25.4 mm in diameter(D), each assembled using 10 unit rods made of Acetal resin (a type of plastic material). It should be noted that the diameter of the test rod is larger than the diameter of the fuel rod (i.e., 9.5 mm). This scale-up of the rod diameter is to more accurately measure the flow field in narrow gap region between the rods by the PIV system. Downstream of the mixing-vane grid, transparent FEP (Fluorinated Ethylene-Propylene) tubes with a length of 200 mm have been placed, each filled with water. As the refractive index of the FEP material (1.34) is quite similar to that of water (1.33), the optical distortion of the laser sheet through the FEP tube filled with water can be minimized. The rod supports are made of stainless steel (SS304) of 5 mm thickness, and have been precisely machined using the EDM (Electrical Discharge Machining) wire cutting process.

Figure 5 shows the cross-sectional view and measured region in the central subchannel of a 4x4 rod bundle with a mixing-vane grid. A 3D printing process was used to manufacture the twist-vane grid which was configured to generate a swirl and crossflow. The material of the spacer grid is ABS (Acrylonitrile butadiene styrene), and its thickness is 1.51 mm and 2.02 mm. The spacer grid has been coated with black paint to minimize light reflection.

The mean and root-mean-square (RMS) lateral velocity was measured using the PIV system in the central subchannel. The PIV measurements were taken at 1.4D, 3D, 6D, 10D, 14D and 20D downstream of the vane grid. The mean and RMS axial velocity were also measured using the LDV

system in the center and rod-to-rod gap of the central subchannel. The LDV measurements were taken from 1.6D (40 mm) to 9.1D (230 mm) downstream of the vane grid. The origin of the axial coordinate (z), i.e., z=0, is placed at the top end of the vane grid. The origin of lateral coordinates (x and y) is defined at the center of the central subchannel. The average flow velocity (Wo) of water in the test bundle is 1.5 m/s at room temperature.

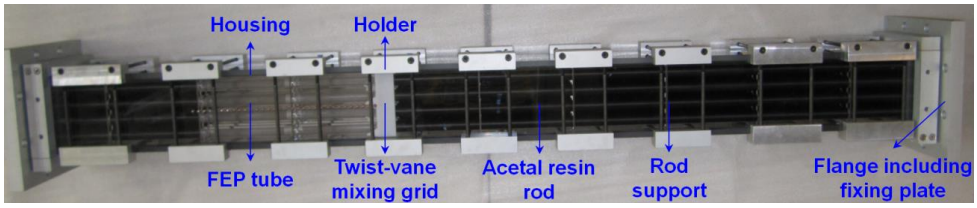

Figure 4: Test section of 4x4 rod bundle with the mixing-vane grid.

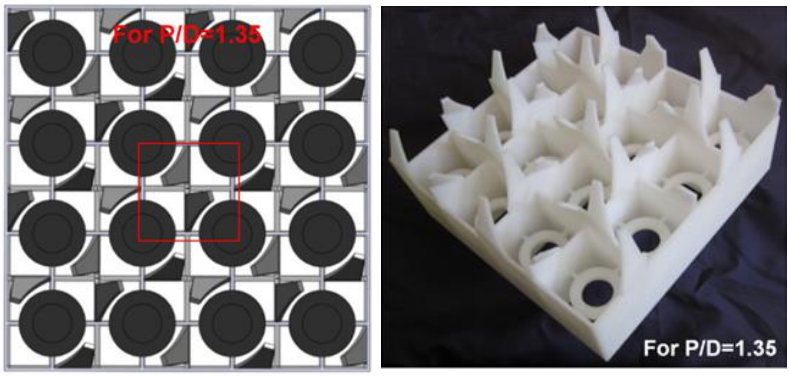

Figure 5: Cross-sectional view of measurement region in 4x4 rod bundle and the mixing-vane grid.

2.2 Heat-transfer Experiment

A heat transfer experiment was carried out in the flow mixing test loop, OFEL, in order to measure the wall temperature of a heated rod. The test section consists of a 4x4 rod bundle with a single heated rod in one of the four central rod positions. Figure 6 shows a schematic of the test section with a heated rod, rod support grid, and twist-vane grid. It indicates the initial elevation of the thermocouples in the test bundle just upstream of the twist-vane grid (z/D = -2.6). To measure the temperature distribution around the heated rod downstream of the vane grid, the heated rod assembly was simply moved upward along the axis, and then fixed at the target axial locations (i.e. z/D = 1.5, 2.0, 2.5, 3.0, 5.0, 10.0 and 12.0). The temperature measurements were then taken.

The design of the heated section is shown in more detail in Figure 7. One 90° quadrant of the heated, stainless steel tube section had five slots machined into it around the circumference to accommodate thermocouples for measuring the rod-wall surface temperature. These slots were machined very precisely and each is 1 mm in width, 1 mm in depth, and 5 mm in length. T-type thermocouples of diameter 1 mm were welded carefully into these slots, and their lead wires pulled out through the gap between the steel/copper tubes and the central copper rod, the rod and tubes electrically insulated from each other by the Teflon sleeve.

The experimental conditions for this thermal bundle test are summarized as follows.

- Bundle average flow velocity: 1.5 m/s
- Heat flux in outer surface (Joule heating): 104 kW/m^2
- Number of samples taken to obtain averaged temperature data: 150
  (The time interval between measurements is 1 second)
- The inlet temperatures (measured at the inlet of the test section) vary from 11 ^{o}C to 14 ^{o}C, depending on the axial position of the heated section

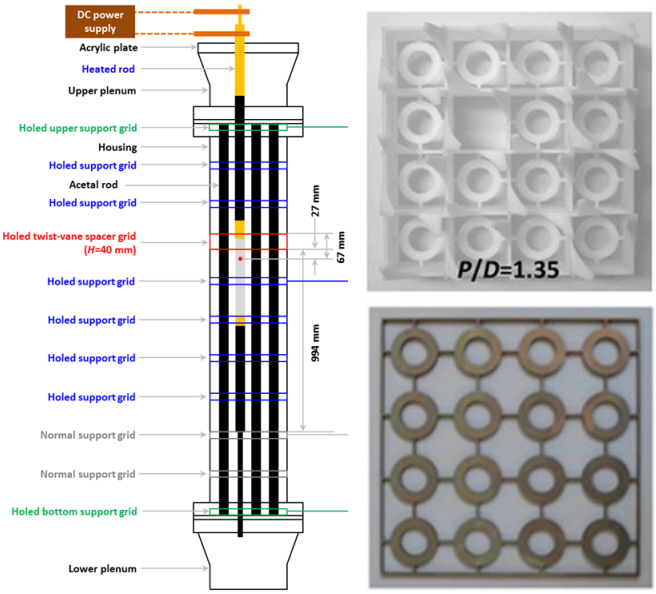

Figure 6: Schematic of heated test section, rod support grid and twist-vane grid.

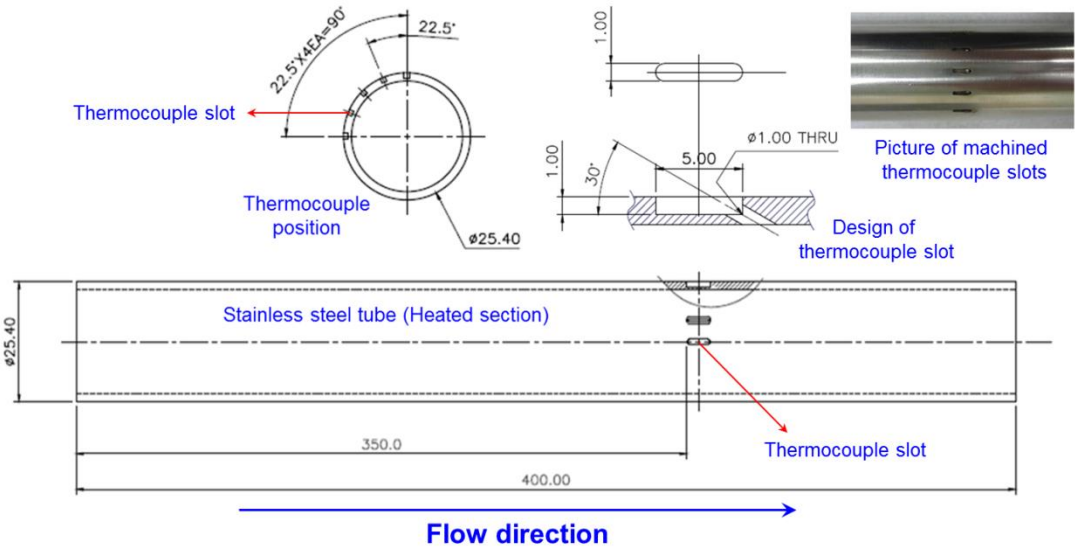

Figure 7: Design of heated section with five thermocouples.

3 CFD Simulation of Rod Bundle Experiments

A CFD analysis is performed to simulate the isothermal and thermal bundle experiments using a 4x4 rod bundle with the twist-vane grid. Figure 8 shows the axial and cross-sectional views of CFD model for the 4x4 rod bundle. The total length of the CFD model is 3 m (1 m upstream and 2 m downstream of the twist-vane grid). The cross-sectional view explicitly shows the twist-vane pattern and finite thickness of a grid plate and mixing vane. The working fluid (water) flows upward parallel to the rod and passes through the mixing-vane grid. The flow field in central subchannel is predicted and compared with the experimental results.

The tetrahedral and polyhedral meshes were generated in the grid region and extruded in the upstream and downstream directions. Figures 9 and 10 illustrate the tetrahedral mesh and polyhedral

mesh, respectively. They show a fine mesh in the vane-grid region and coarse mesh away from the vane grid. Five prism layers are created near the rod surface and housing wall in order to more accurately simulate boundary layer. The total number of mesh cells is changed from 25 million cells to 73 million cells.

A uniform flow (1.5 m/s) and constant water temperature are used at the inlet boundary. A constant pressure is applied at the outlet boundary, and a no-slip condition is applied at the rod wall and the bundle housing. A constant heat source is given to a single heated rod which simulates the direct heating experiment. The turbulence models based on the Reynolds-averaged Navier-Stokes (RANS) equation are used to simulate the flow turbulence in a rod bundle.

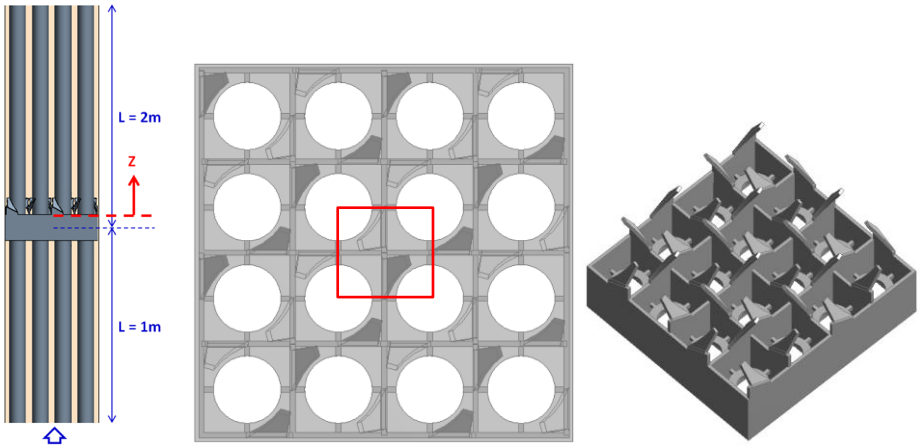

Fig. 8: CFD model for 4x4 rod bundle with twist-vane grid.

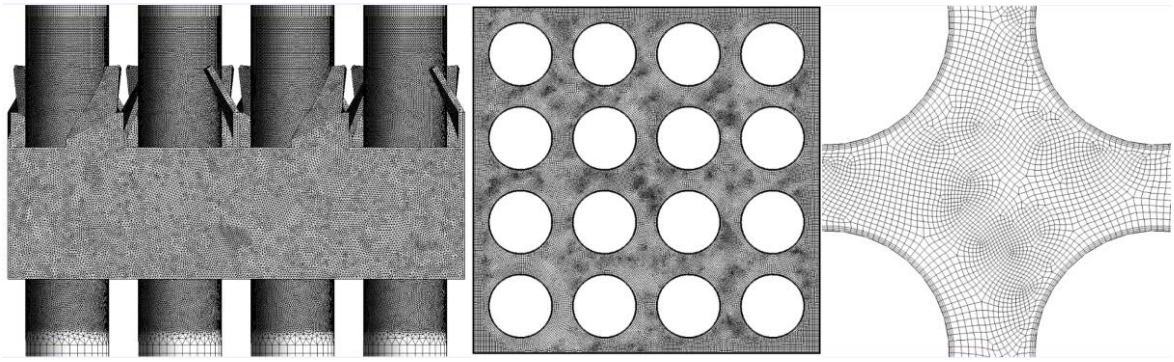

Fig. 9: Tetrahedral mesh for 4x4 rod bundle with twist-vane grid.

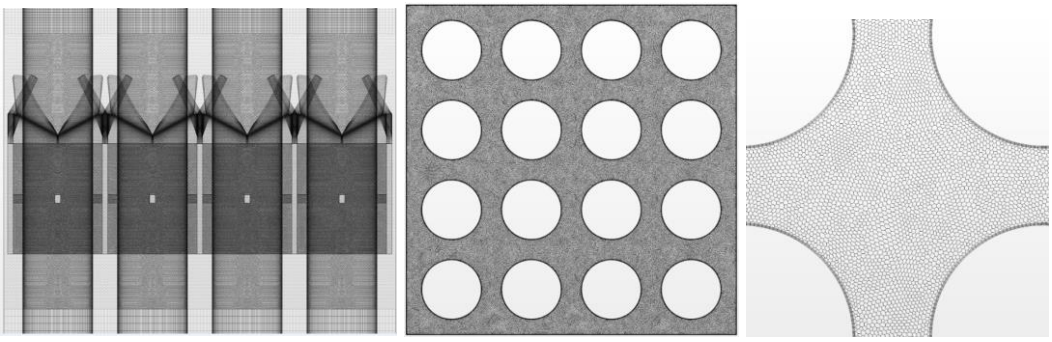

Fig. 10: Polyhedral mesh for 4x4 rod bundle with twist-vane grid.

The commercial CFD codes ANSYS CFX 18.0 [13] and STAR-CCM+ 11.0 [14] were used to perform a CFD analysis. Because the overall Reynolds number for the experimental conditions is 40,000, the RANS turbulence models (standard k-e model, RNG k-e, Realizable k-e, SST model) were used to simulate the flow turbulence. The CFD calculation was continued until the normalized residuals of governing equations are lower than 1.E-04 and a monitored velocity downstream of the vane grid is practically constant.

The grid convergence test was performed using three different meshes, e.g., 25 million cells (mesh 1), 50 million cells (mesh 2), and 73 million cells (mesh 3). The base cell size ranges from 0.7 mm to 2 mm and the number of cell points in a circular boundary (fuel rod) is 72, 90, and 144 for mesh 1-3, respectively. Figure 11 shows the lateral velocity profile along the horizontal centerline of the central subchannel and the streamwise variation of axial velocity at the subchannel gap. Mesh 2 appears to be acceptable, but mesh 3 shows double peaks of lateral velocity well near downstream of vane grid (i.e., z/D=1.4), which was observed in the experiment. Hence, mesh 3 is selected as the optimum case for this CFD simulation. The non-dimensional distance from the rod surface to the first cell (y_w^+) is 10-15 in the outlet boundary.

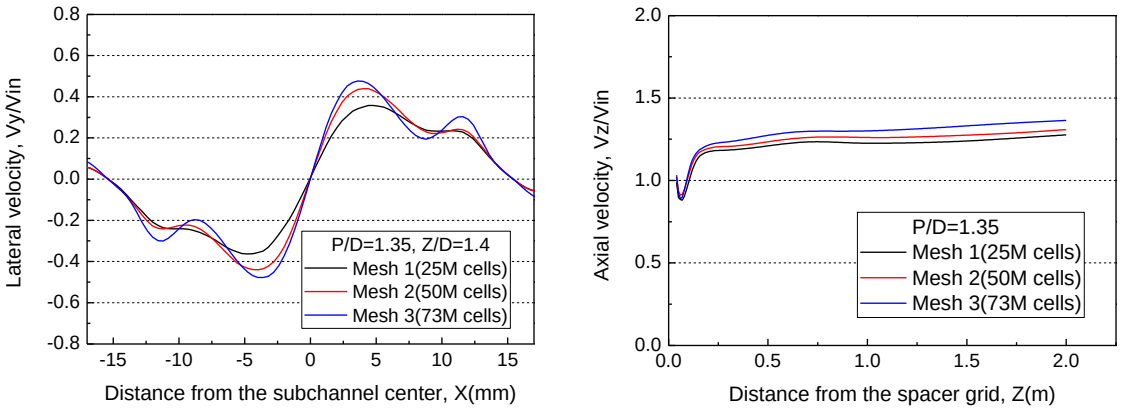

Fig. 11: Grid convergence test for CFD meshes.

4 Results and Discussion

4.1 Flow Mixing in Rod Bundle

The CFD simulation of the isothermal bundle test predicted the flow mixing patterns upstream and downstream of the mixing-vane grid in a 4x4 rod bundle. Figure 12 shows the CFD prediction of the velocity contour far upstream (z=-500 mm) and near downstream (z=36 mm) of the vane grid. At the far upstream location, the velocity is high in the core region of the subchannel and low in the gap region between the rods. Because there is neither swirl nor crossflow upstream of the vane grid, the flow mixing in the rod bundle is insignificant. However, the velocity contour near the downstream of the vane grid shows a strong swirl in the subchannel and crossflow between the neighboring subchannels. The mixing-vane grid significantly enhances the flow mixing in the rod bundle by generating a swirl and crossflow.

Figure 13 compares the flow mixing pattern in the central subchannel near the downstream of the mixing vane, which was obtained through a PIV measurement and the CFD method. The experimental and CFD results show a large elliptic swirl in the core region and high crossflow in the gap region. They also show a secondary swirl in the peripheral region near the gap. The CFD analysis predicts the flow mixing pattern downstream of the vane grid which agrees well with the experimental results. Further downstream of the mixing-vane grid, the flow mixing pattern shows a single circular swirl in the central region and an asymmetric crossflow in the gap region. The magnitude of swirl and crossflow decreases significantly far downstream of the vane grid.

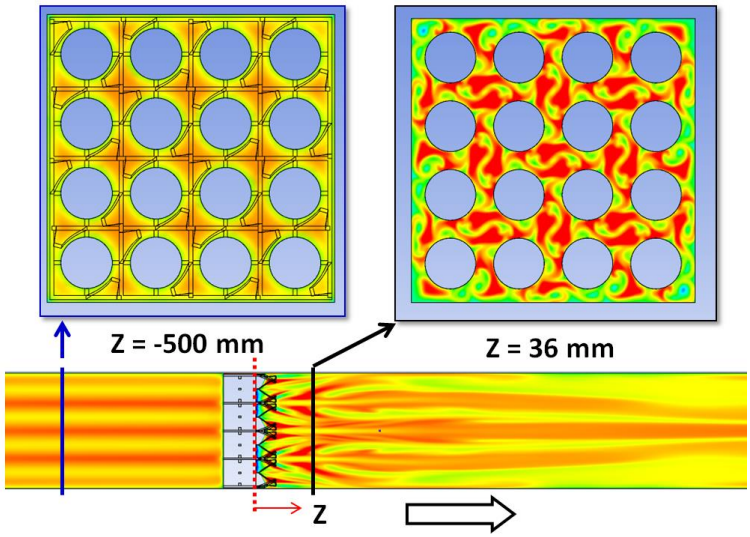

Fig. 12: Flow distribution in 4x4 rod bundle with the mixing-vane grid.

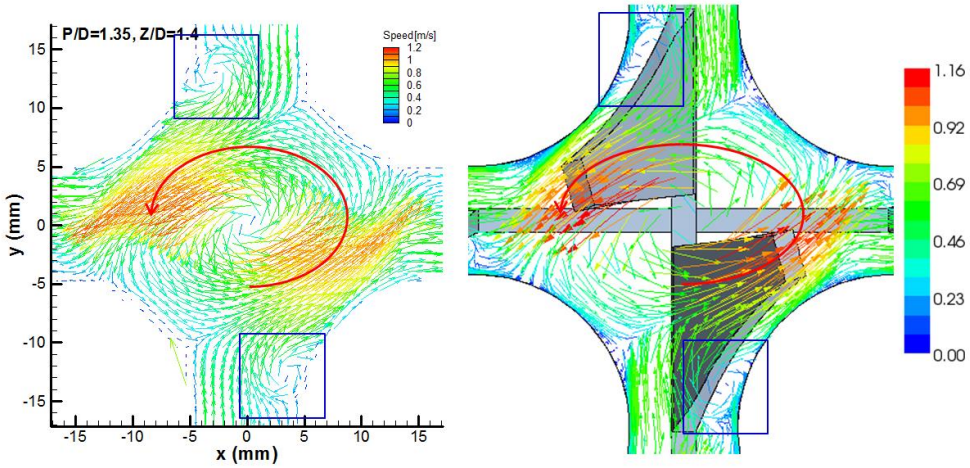

Fig. 13: Flow mixing pattern in the central subchannel near downstream of the mixing-vane grid; (left) experiment, (right) CFD method.

Figure 14 shows a comparison of the axial mean velocity (Wm) in the center and gap of the central subchannel. The experiment shows a slight decrease in axial velocity in the center near the downstream (i.e., z/D < 2) and increases to an asymptotic value further downstream. The minimum and maximum velocity is 1.3 m/s (87% of bundle average velocity, Wo) and 2 m/s (1.33 Wo), respectively. The SST model and the realizable k-e model in STAR-CCM+ predict the axial velocity profile, which agrees well with the experimental results. The SST model in the CFX shows a smaller variation of the axial velocity. The RNG k-e model in the CFX predicts the variation in axial velocity, showing a good agreement with the experimental profile, but at a location a little further downstream of the minimum velocity. The location of the minimum axial velocity in the center is 1.5D for the experiment, and 1.5D, 2D and 2.5D for the SST model (CCM+), the realizable model (CCM+), and the RNG model (CFX), respectively.

The measured axial mean velocity in the gap shows double peaks near the downstream of the vane grid and decreases to a constant value far downstream. The peak velocity is 2.1 m/s (1.4 Wo), and the far downstream velocity is 1.7 m/s (1.13 Wo). The CFD predictions also show double peaks in the axial velocity profile and decrease to an asymptotic value. Even if the CFD calculations show somewhat under-predictions, they agree reasonably with the experimental results. Hence, the overall agreement between the CFD prediction and the experiment is reasonably good for the axial mean velocity.

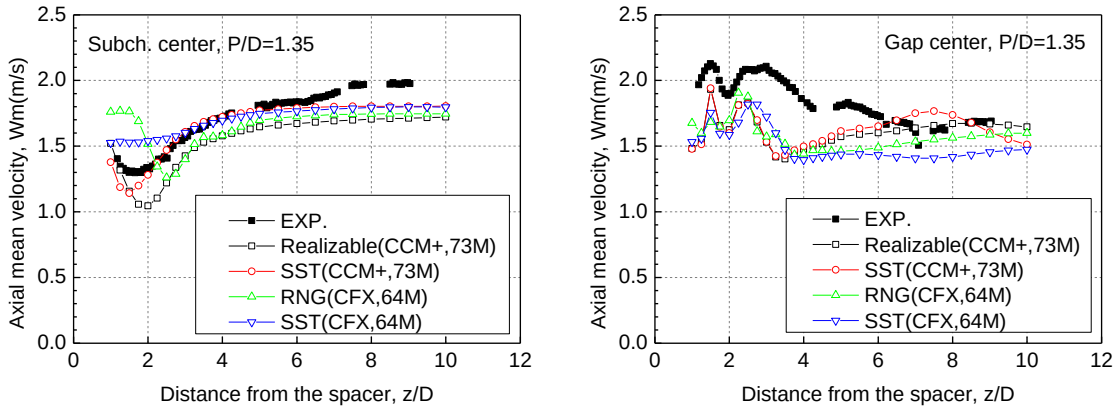

Fig. 14: Comparison of axial mean velocity: (left) subchannel center, (right) gap center.

Figure 15 compares the variation of axial RMS velocity (Wrms) downstream of the mixing-vane grid in the center and the gap of the central subchannel. The RMS velocity is obtained through the following definitions for the experiment and the CFD calculation. Because the CFD calculation used two-equation turbulence models, the RMS velocity for the CFD method is indirectly calculated from the turbulent kinetic energy assuming isotropic turbulence.

$$W_{rms}(EXP) = \sqrt{\frac{\sum_{i=1}^{N}\left(W_i - \overline{W}\right)^2}{N-1}}$$

$$W_{rms}(CFD) = \sqrt{\frac{2k}{3}}$$

Where,

W_i – instantaneous velocity in axial (streamwise) direction
$\overline{W}$ – mean axial velocity
N – number of sampled data
k – turbulent kinetic energy

The axial RMS velocity in the subchannel center tends to decrease gradually as it goes away from the spacer grid. The measured RMS velocity is 0.4 m/s (26% Wo) at z/D=1 and 0.2 m/s (13% Wo) at z/D=10. The CFD predictions show a large discrepancy between turbulence models as well as the experiment particularly in the near downstream region, e.g., 0 < z/D < 3. The realizable k-e model in the STAR-CCM+ and RNG k-e models in CFX predict a significantly lower RMS velocity near the downstream (i.e., z/D=2) than the measured one. The SST model in the STAR-CCM+ predicts a slight peak of RMS velocity at z/D=2. The SST model in CFX predicts the gradual decrease of the RMS velocity which shows the downstream variation similar to the experimental data. However, the CFD predictions of RMS velocity in the subchannel center are almost 50% lower than the experimental result.

The axial RMS velocity in the gap appears to show a secondary peak at z/D=2 in the experiment and at z/D=3 in the CFD predictions (Realizable k-e and SST models). The RNG k-e model in CFX predicts a significantly lower RMS velocity than other turbulence models, as well as the experiment in near the downstream region (z/D < 2). The measured RMS velocity in the gap is 0.3 m/s (20% Wo) near the vane grid and 0.15 m/s (10% Wo) far downstream. The predicted RMS velocity in the gap is 0.2 m/s (13% Wo) near downstream and 0.1 m/s (7% Wo) far downstream. The CFD predictions of the RMS velocity in the gap are 30% lower than the experimental results. Hence, the overall discrepancy between the CFD prediction and the experiment is somewhat large for an axial RMS velocity.

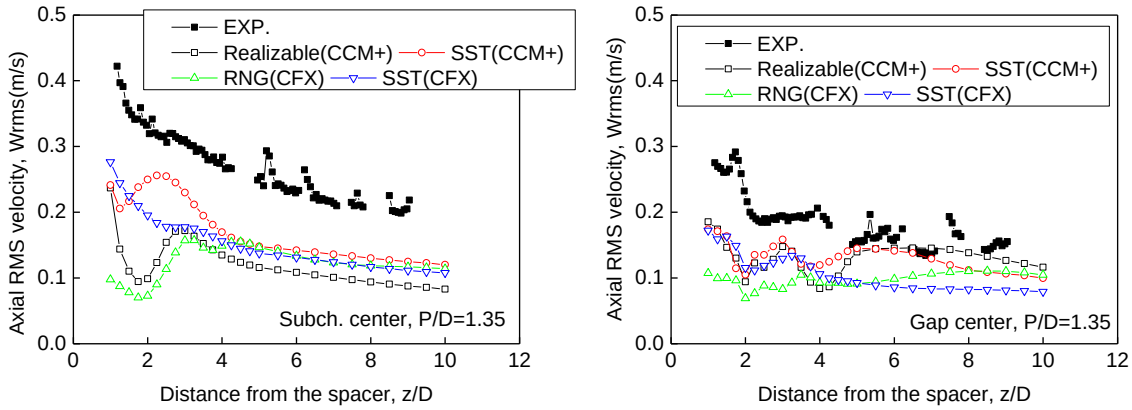

Fig. 15: Comparison of axial RMS velocity: (left) subchannel center, (right) gap center.

The lateral mean velocity (Vm) in the central subchannel is compared in Figure 16 for the two downstream locations, i.e., z/D=1.4 and z/D=10. The lateral velocity is defined as a velocity component in the vertical direction from the horizontal centerline. Because the mixing vane on the spacer grid generates a clockwise swirl in the central subchannel, the lateral velocity is positive on the right side (i.e., x > 0) and negative on the left side (i.e., x < 0).

The lateral velocity distribution at z/D=1.4 shows a symmetric profile with double peaks about the center of the subchannel, i.e., x=0. The maximum lateral velocity is 0.7 m/s (46% Wo). The realizable k-e and SST models predict the lateral velocity profile, showing an excellent agreement with the experimental one. The RNG k-e model in CFX gives a somewhat larger variation of lateral velocity near the center, i.e., x = -2 & 2 mm.

The lateral velocity distribution at z/D=10 also shows a symmetric profile with a single peak. The maximum lateral velocity is 0.5 m/s (33% Wo). The single peak occurs near the center (i.e., x = -5 & 5 mm) for the experiment and a little away from the center (i.e., x = -7 & 7 mm) for the CFD predictions. The CFD predictions of all turbulence models agree well with the experimental results.

In summary, this CFD simulation predicted a large swirl and crossflow in the rod bundle with the mixing-vane grid which agree well with the experimental observation. The CFD analysis predicted the axial mean velocity which agrees reasonably with the experiment. However, the discrepancy between the CFD prediction and the experiment is somewhat large for the axial RMS velocity. The CFD prediction of the lateral velocity agrees well with the PIV measurement. In particular, the realizable k-e and SST models predict the lateral velocity profile showing an excellent agreement with the experimental one.

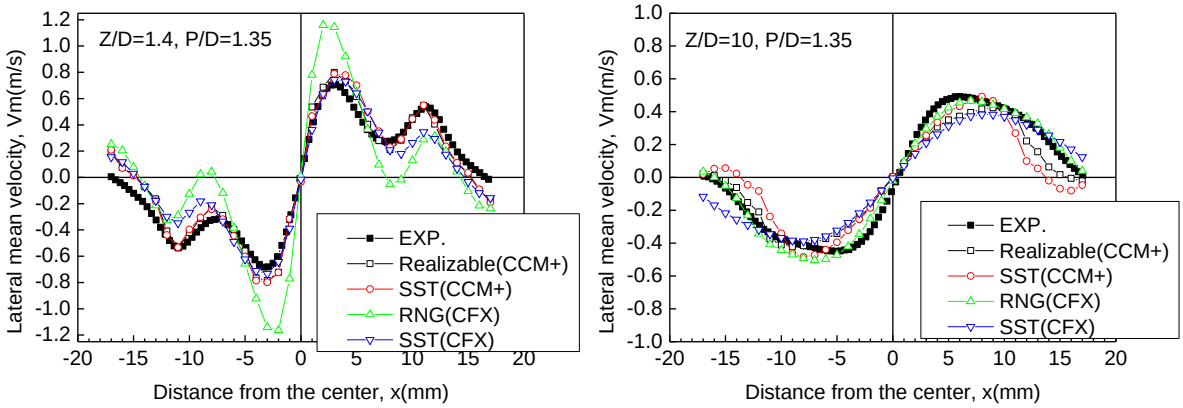

Fig. 16: Comparison of lateral mean velocity for (left) near downstream (z/D=1.4), and (right) far downstream (z/D=10).

4.2 Heat Transfer in Rod Bundle

A preliminary CFD analysis was performed to examine the thermal boundary condition in a heated rod. A constant heat flux was used in the outer or inner surfaces, and the constant heat source was also examined. Figure 17 shows the effects of the heating condition on the wall temperature in a heated rod. The heat source and heat flux in the inner surface show an identical distribution of the wall temperature. It should be noted that the heat source and heat flux in the inner surface were calculated from the heat flux in the outer surface (104 kW/m^2) using geometry data. The heat flux in the outer surface gives the wall temperature slightly lower than the cases for the heat source and heat flux in the inner surface. Because the thermal boundary condition with heat source is similar to the Joule-heating condition in the thermal bundle test, this CFD analysis used a constant heat source in a heated rod for the thermal boundary condition.

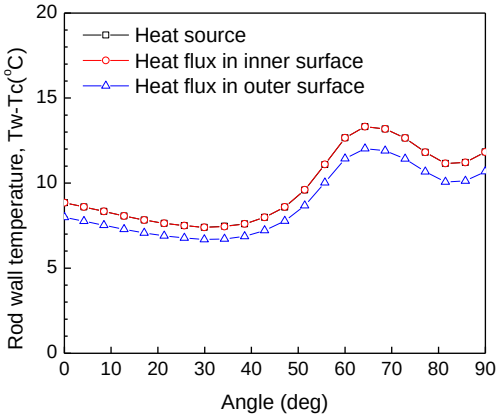

Fig. 17: Effects of heating condition in heated rod for CFD analysis.

Figure 18 shows the CFD prediction of the wall temperature in a heated rod using the realizable k-e model. The CFD prediction indicates the overall decrease in wall temperature (i.e., heat transfer enhancement) downstream of the mixing-vane grid. However, there are hot spots observed in a heated rod downstream of the vane grid owing to the non-uniform flow mixing, such as a secondary swirl, as shown in Fig. 13. The minimum and maximum wall temperatures are 17.9 °C and 26.3 °C, respectively.

Figure 19 shows a cross-sectional view of the velocity and temperature contour at a nearby location and a little farther downstream, e.g., z/D=1.5 and 10. The CFD prediction shows a non-uniform distribution of the heated rod temperature in the circumferential direction. A high rod and fluid temperature is predicted in a low flow region where the swirl and crossflow changes in direction. The location of the hot temperature varies in the axial location downstream of the vane grid because the flow mixing pattern changes. It should also be noted that a hot fluid zone is large in the near downstream location (z/D=1.5) owing to a high swirl and crossflow.

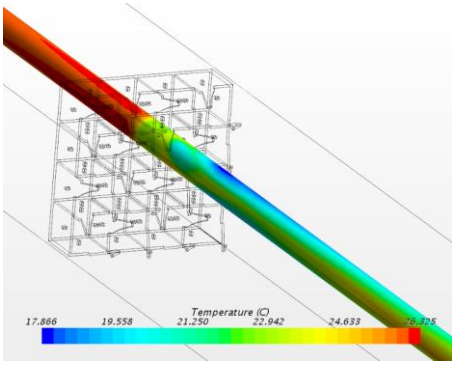

Fig. 18: Wall temperature in heated rod through CFD analysis

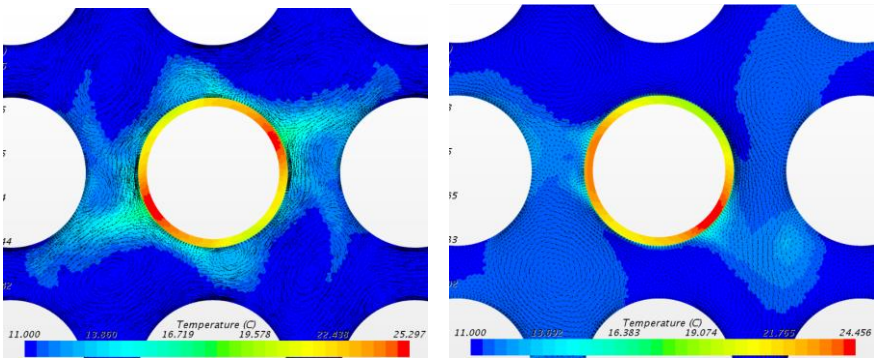

Fig. 19: Velocity and temperature contours downstream of the mixing-vane grid: (left) z/D=1.5, (right) z/D=10

The circumferential variation of rod temperature at z/D=1.5 is compared in Figure 20 to show the effects of the mesh type and turbulence model. It should be noted that the rod temperature is expressed as the temperature difference between the wall (outer surface of heated rod) and fluid. The CFD predictions show a large discrepancy with the measured one in a narrow gap region, i.e., $80 < \theta < 90$. The realizable k-e and SST models appear to predict the wall temperature variation which reasonably agrees with the experimental results. The standard k-e model in CFX shows a larger temperature variation than the standard k-e model in STAR-CCM+ as well as the measured one. It should be noted that the CFX and STAR-CCM+ used a tetrahedral mesh and polyhedral mesh, respectively.

Figure 21 compares the experimental results and predictions of wall temperature in a heated rod at z/D=10 using CFX and STAR-CCM+. The CFD predictions show a wall temperature significantly lower than the measured one. The experimental data show the minimum temperature of 14 ^{o}C at θ=22.5 and the maximum temperature of 18 ^{o}C at θ=67.5. However, the RNG k-e model in CFX predicts the minimum and maximum temperature of 7 ^{o}C at θ=30 and 12 ^{o}C at θ=67.5. The standard k-e model in CFX shows the temperature variation similar to the RNG model with 1 ^{o}C lower. The SST model in CFX gives the maximum temperature at θ=90, which is different from other turbulence models. Hence, it can be said that the RNG and standard k-e models in CFX predict the circumferential position of cold and hot spots, which agrees well with the experimental results. However, the standard and realizable k-e models in STAR-CCM+ predict the maximum temperature at θ=90, while the SST model in STAR-CCM+ gives a maximum value at θ=65. There is no large difference between the standard k-e model and realizable k-e model in STAR-CCM+. The SST model in STAR-CCM+ seems to give a better prediction than the standard and Realizable k-e models. It should also be noted that the mesh type (tetrahedral vs. polyhedral) has a large influence on the CFD prediction of wall temperature in a rod bundle.

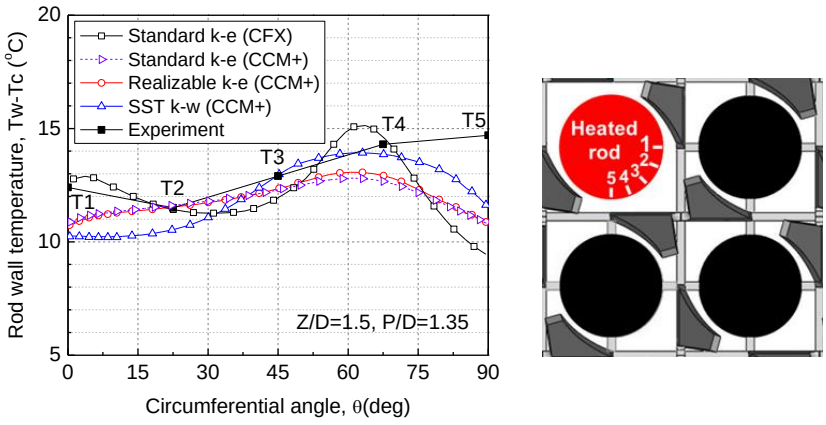

Fig. 20: Comparison of circumferential wall temperature in heated rod at z/D=1.5

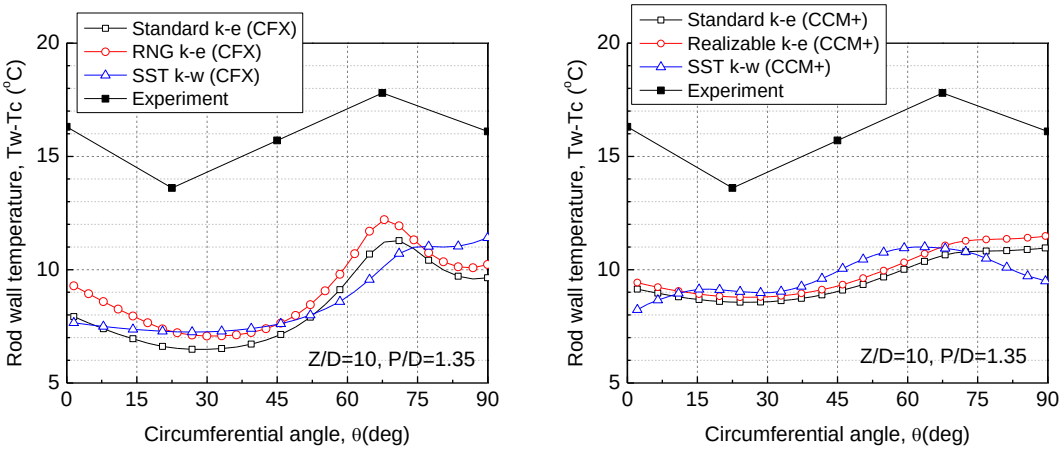

Fig. 21: Comparison of circumferential wall temperature in heated rod at z/D=10 depending on the turbulence model and mesh type(tetrahedral in CFX vs. polyhedral in STAR-CCM+)

The axial variation of wall temperature in streamwise direction is compared in Figure 22, depending on the turbulence model and mesh type. The CFD predictions and experimental data show a decrease in wall temperature near the downstream of the mixing-vane grid which indicates the heat transfer enhancement. The minimum wall temperature occurs at z/D=5 and z/D=3 for the CFD predictions and experiment, resepctively. The CFD calculations predict the wall temperature significantly lower than the experimental result for the far downstream location, i.e., z/D > 5. The standard and realizable k-e models in STAR-CCM+ give almost the same predictions. The SST model in STAR-CCM+ predicts the lowest wall temperature at z/D=5 (highest enhancement in heat transfer). The RNG k-e model in CFX also predicts the larger wall temperaure drop downstream of the vane grid, which means a higher heat transfer enhancement. The difference between the minimum and maximum wall temperatures is 3.5 °C and 4-5 °C for the experiment and CFD prediction, respectively. Because the maximum wall temperature upstream of the vane grid with respect to the fluid temperature is 16 °C for the experiment and 12 °C for the CFD prediction, the heat transfer enhancement by the mixing vane can be estimated as 22% and 37% for the experiment and CFD prediction, respectively.

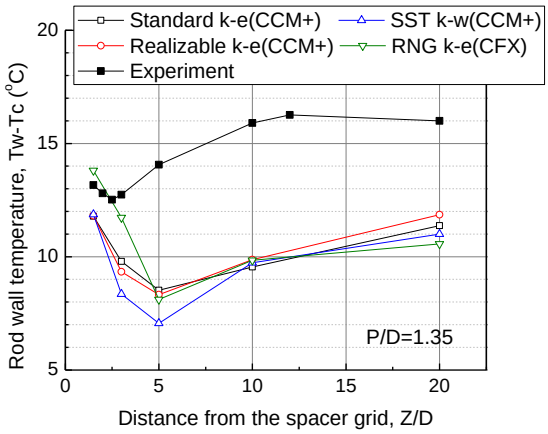

Fig. 22: Axial variation of wall temperaure depending on turbulence model and mesh type

5 Conclusion and Future Work

A CFD analysis was conducted to study the applicability of the CFD method in predicting the flow

mixing and heat transfer in a nuclear fuel assembly, which is a rod bundle with a mixing-vane grid. The isothermal and thermal experiments in a 4x4 rod bundle were simulated in this CFD study. The CFD simulation of isothermal bundle test predicted the flow mixing in a rod bundle owing to a large swirl and crossflow caused by a mixing-vane grid, which agree well with the experimental observation. The CFD analysis predicted axial and lateral mean velocities that agree reasonably with the experimental results. However, the CFD analysis predicted the axial RMS velocity significantly lower than the measured one.

The CFD simulation of thermal bundle test predicted a high temperature near the heated rod, and the heat is propagated into adjacent subchannels owing to flow mixing induced by the mixing-vane grid. Cold and hot spots are predicted in a heated rod downstream of the vane grid owing to a non-uniform flow mixing. The CFD analysis using Realizable k-e and SST models predicted the wall temperature variation near the vane grid, which agrees reasonably with the experimental results. However, the CFD predictions of the wall temperature far downstream are significantly lower than the measured one. It should also be noted in a thermal bundle simulation that the mesh type (tetrahedral vs. polyhedral) has a large effect on the circumferential variation of the wall temperature. Hence, future work is necessary to investigate the effects of a turbulence model and mesh type, particularly for a far downstream heat transfer in a thermal bundle simulation.

Nomenclature

D	Diameter of test rod (m)
P	Pitch of rod array (m)
T_w	Wall temperature in heated rod (^oC)
T_C	Fluid (water) temperature (^oC)
Vm	Lateral mean flow velocity in the subchannel (m/s)
Wo	Average flow velocity in rod bundle (m/s)
Wm	Axial mean flow velocity in the subchannel (m/s)
Wrms	Axial root-mean-square(RMS) velocity in the subchannel (m/s)
z	Axial distance from the mixing-vane grid in streamwise direction (m)
θ	Circumferential angle (deg)

Acknowledgement

This work was supported by the National Research Foundation in Korea (NRF-2017M2A8A5015064) funded by the Korean government, Ministry of Science and ICT (MSIT), and the cooperation project between KAERI and CIAE.

References

[1] Shen Y. F., Cao Z. D., Liu Q. G., An investigation of crossflow mixing effect caused by grid spacer with mixing blades in a rod bundle, Nuclear Engineering and Design, 125(2): 111–119, 1991.

[2] Yang S. K., Chung M. K., Spacer grid effects on turbulent flow in rod bundles, Journal of Korean Nuclear Society, 28:56–71, 1996.

[3] McClusky H. L., Holloway M. V., Beasley D. E., Conner M. E., Development of swirling flow in a rod bundle subchannel, Journal of Fluids Engineering, 124(3): 747-755, 2002.

[4] McClusky H. L., Holloway M. V., Conover T. A., Beasley D. E., Conner M. E., Smith L. D., Mapping of the lateral flow field in typical subchannels of a support grid with vanes, Journal of Fluids Engineering, 125(6): 987-996, 2004.

[5] Karoutas Z., Gu C. Y., Scholin B., 3-D flow analyses for design of nuclear fuel spacer, *Proc. 7th Int. Mtg. Nuclear Reactor Thermal-Hydraulics (NURETH-7)*, New York, USA, 1995.

[6] Imaizumi M., Ichioka T., Hoshi M., Teshima H., Kobayashi H., Development of CFD method to evaluate 3-D flow characteristics for PWR fuel assembly, *Transaction of 13th Int. Conf. Structural Materials in Reactor Technology (SMiRT)*, Porto Alegre, Brazil, 1995.
[7] In W. K., Numerical study of coolant mixing caused by the flow deflectors in a nuclear fuel bundle, Nuclear Technology, 134(2): 187-195, 2001.
[8] Holloway M. V., McClusky H. L., Beasley D. E., Conner M. E., The effect of support grid features on local, single-phase heat transfer measurements in rod bundles, Journal of Heat Transfer, 126(1): 43-53, 2004.
[9] Holloway M. V., Conover T. A., McClusky H. L., Beasley D. E., Conner M. E., The effect of support grid design on azimuthal variation in heat transfer coefficient for rod bundles, Journal of Heat Transfer, vol. 127(6): 598-605, 2005.
[10] Conner M. E., Smith III L. D., Holloway M. V., Beasley D. E., Heat transfer coefficient testing in nuclear fuel bundles with mixing vane grids, Water Fuel Performance Meeting, Kyoto, Japan, 2005.
[11] W.K. In, C.H. Shin, C.Y. Lee. Experimental observation of forced flow mixing in tight-lattice rod bundle, Transaction of the American Nuclear Society, 110:662-664, Reno Nevada, USA, 2014.
[12] W.K. In, C.H. Shin, C.Y. Lee. Convective heat transfer experiment of rod bundle flow with twist-vane spacer grid, Nuclear Engineering and Design, 295: 173-181, 2015.
[13] ANSYS Inc., User guide for ANSYS CFX-18.0, 2017.
[14] CD-Adapco, User guide for STAR-CCM+ release 11.0, 2017.